Daniel's Super Cool and overly long title

Daniel Mortensen, Jacob Gunther

***Abstract*—TODO: add abstract**

***Index Terms*—TODO: Add Keywords**

I. Introduction

Recent calls for a reduced carbon footprint have pushed transit authorities to adopt battery electric buses (BEBs). Conversion from diesel and CNG to BEB reduces environmental impact [21] as BEBs provide zero emissions and access to renewable energy [14].

These benefits are possible because BEB draw power from electrical infrastructure. The loads introduced by charging are substantial and can exceed the grid capacity [17][6][3], requiring prohibitively expensive upgrades. The cost of upgrading is reflected in the billing structure used by power providers and can make large-scale charging undesireable for consumers.

One approach to reducing charge costs is to defer upgrades by efficiently managing when and at what rates buses charge. However, developing charge plans must consider a number of factors. All buses must maintain a minimum charge level while adhering to route schedules. When charging, batteries must have sufficient charge time and share a limited number of chargers. All charging must also be done while other services draw power from the grid, acting as uncontrolled loads. The focus of this work is to find an optimal charge schedule which meets these requirements and minimizes the cost of grid use in the presence of uncontrolled loads. This problem is refered to hereafter as the 'charge problem'.

The remainder of this paper is organized as follows: Section II describes related work and Section III outlines a graph-based framework for modeling the operations environment. Section IV extends the content of III to account for differences between day and night operations, and Section V incorporates the problem constraints involving battery charge dynamics. Sections VI and VII translate the rate schedule used for billing and into an objective function to minimize. Finally, Sections VIII, IX, and X briefly describe the optimization software used to solve the resulting mixed integer linear program developed in previous sections, presents results, and describes future work.

II. Literature Review

This section summarizes prior work related to the charge problem and includes discussion on battery charging and managing runtime costs. The final subsection discusses the contributions of this paper, and how they relate to prior methods.

A. Battery Charging

The refueling process for BEBs takes longer then the process for diesal and CNG buses [18]. A diesal or CNG engine can refuel in several minutes but an electric bus may require up to several hours, making the extended charge time a primary deterrent in converting to BEBs.

To circumvent long refuel times, [20] and [11] propose an approach which replaces batteries when the state of charge is low. The exchange would replace the current battery with one that was fully charged and return spent batteries to recharge afterward. Exchanging batteries would reduce down time, but is non-trivial because the replacement requires specialized tools and/or automation.

Another alternative is to inductively charge buses as they move about. Dynamic charging would simplify logistics because it eliminates the need to stop and recharge. Both [2] and [12] propose methods that inductively charge BEBs using specialized hardware in the road. A technique developed by [5] provides a planning framework for charger placement that maximizes the benefits of dynamic charging. Unfortunately, inductive charging requires infrastructure which may not be available and is costly and disruptive.

Refueling BEBs in a charge station allows buses to charge in the traditional sense and only requires an intelligent charge schedule. Following a charge schedule requires minimal infrastructure and utilizes native charge ports in the BEBs with no need for additional tools or automation. Planning algorithms use foreknowledge of the runtime environment and battery dynamics to identify when, and to which buses chargers should connect. Planning algorithms discussed in this review are considered on a scale from 'reactive' to 'global', where reactive methods focuse only on the present, and global techniques use knowledge about the operating environment to form a plan.

Because reactive planning tend to focus on presential circumstances, they require minimal knowledge of the operational environment, making them extremely versatile. Methods of this type are both computationally efficient and adapt to many use cases. One such example is illustrated in [4], which splits the total power draw between the grid and an external battery to regulate the instantaneous load.

Reactive algorithms can be enhanced by encoding details for future events to improve decision making. If only event details within a finite horizon are used, the algorithm becomes a hybrid, containing elements from both reactive and global techniques. For example, [1] describes a technique for optimizing a charging schedule up to a scheduling horizon. Changing the horizon adjusts both the scope and computational complexity of the solution. In stochastic environments, a smaller window would be beneficial as charge schedules must be frequently

recomputed, whereas in more stable circumstances, a larger window size would yield higher performance.

When an algorithm includes information over all time periods, it becomes global. Because global algorithms assume complete foreknowledge of future events, they provide globally optimal plans and give the highest performance. The authors of [10] provide a technique which assumes foreknowledge of the current grid use. The grid schedule is encoded in the algorithm to inform optimal charging periods. Both [19] and [7] assume that bus schedules are known a priori and use this knowledge to stagger charge times and meet operational constraints.

B. Cost Optimization

In addition to charge constraints, This paper focuses on minimizing the cost associated with charging and minimizes over energy charges for on and off-peak, power (or demand) charges for on and off-peak, and facilities charges [16]. Prior work has dealt with charge costs in various ways.

The authors in [8] propose a method to forcast power use. Work done by [15] propose a method which reduces the demand charge by using power forcasts [8] to plan charge times. When forcasting is not possible, both [13] and [4] propose methods that decreases power demand by observing the load and drawing additional power from an on-site battery. Additionally, [7] minimized over on/off peak energy as part of their work.

C. Contributions

This work develops a comprehensive charge schedule planning framework which extends the planner proposed by [19] to include multi-rate charging, uncontrolled loads, night/day charging, and a realistic rate schedule in [16]. Our method formulates the bus charge problem as a Mixed Integer Linear Program (MILP) and is unique because the objective function is the cost for the transit authority and includes charges for on-peak and off-peak energy use, on-peak and off-peak demand, and overall, or facilities, demand. The proposed framework handles contention for charging resources in a globally optimal manner which guarantees charger availability even when chargers are scarse.

Prior work has also made assumptions for night time charge behavior. This work eliminates the need for such by including night charging in the charge schedule. The modeling of night and day charging also includes their respective operational constraints such as charge rates, bus availability, and the number of available chargers.

Our work also seeks to understand how variable rate, as compared to single rate, charging affects the cost optimality. necessary? with the addition of variable charge rates and a more accurate representation of battery charging dynamics.

The final contribution is recognizing that our framework enables transit authorities and power providers to come together and find a mutually beneficial solution that predicts montly costs for transit authorities and infrastructure demand for power providers.

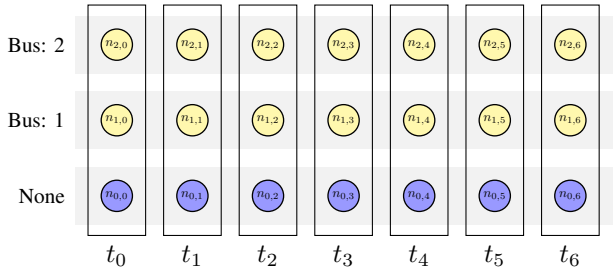

Fig. 1: Graph showing buses and timesteps

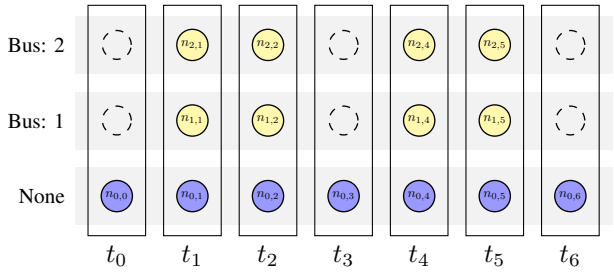

Fig. 2: Bus availability represented in a graph

III. Graph Based Problem Formulation

This section formulates the charge problem as a graph. The first subsection describes the intuition behind this graph-based approach and the second represents the graph as a series of equality and inequality constraints in a Mixed Integer Linear Program (MILP).

A. Graph Formulation

A solution to the bus charge problem must reveal both *when* and *to which* bus a charger should connect, suggesting a model with two dimensions. The first dimension characterizes time and is given discretely in a left to right fashion. The second dimension encodes the charger state and extends vertically as shown in figure 1. The charger may occupy one of several states. It may be connected to one of the N buses, or it may be unconnected, giving a total of $N+1$ charge states. The 2-D representation is encoded as a grid and a node, $n_{i,j}$, can be placed wherever a charge state and time index intersect. These nodes are used to represent a charger in the i^{th} charge state during the j^{th} time index (see figure 1). For example, $n_{1,0}$ from figure 1 represents a state where a charger is connected to Bus 1 at t_0.

However, the presence of nodes at every state-time intersection suggests that buses can always connect. This does not reflect reality because buses cannot connect when they are away from the station. Nodes are therefore only present in the grid when a corresponding bus can connnect to a charger and are absent when a bus leaves the station. Consider the two bus scenario from figure 1 where buses 1 and 2 provide transit services at t_0, t_3, and t_6. The schedule is encoded by removing $n_{1,0}$, $n_{2,0}$, $n_{1,3}$, $n_{2,3}$, $n_{1,6}$, and $n_{2,6}$ to reflect the grid shown in figure 2.

The state of a charger at any time is represented by occupying a corresponding node. Changes in charger state

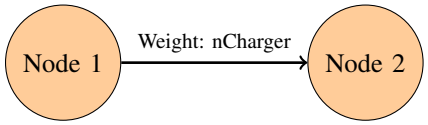

Fig. 3: Node to Node Connection

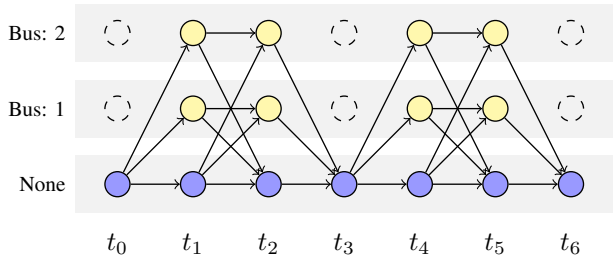

Fig. 4: Graph-based model of the complete decision-space

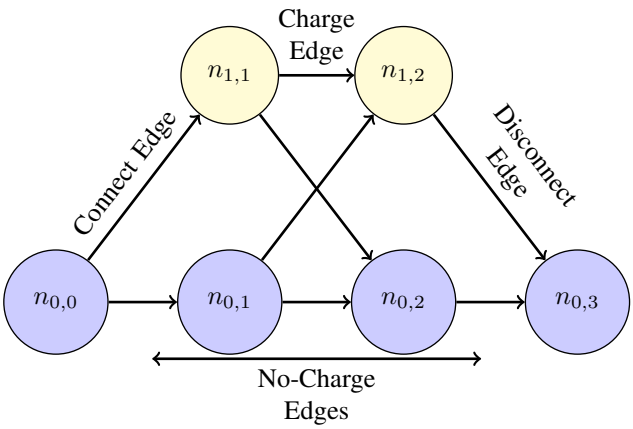

Fig. 5: Connect, Disconnect, and Charge Edges

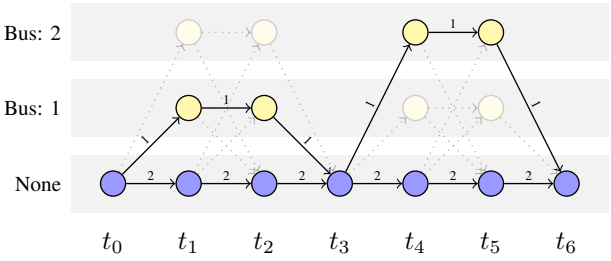

Fig. 6: One solution to a 2-bus 3-charger scenario

and time, are therefore reflected by a transition from one node to the next. These transitions are called edges (see figure 3) and represent decisions to connect to, charge, not charge, or disconnect from buses. An edge's decision is determined by the nodes on either end. Consider the edge from $n_{0,0}$ to $n_{0,1}$ in figure 5. This edge represents a no-charge decision because the nodes on both ends represent a disconnected charge state. Chargers cannot charge while disconnected, so the edge decision is no-charge. Similarly, the edge between $n_{1,1}$ and $n_{1,2}$ indicates a to-charge decision as both $n_{1,1}$ and $n_{1,2}$ represent states where a charger is connected. Both to-charge and no-charge decisions are represented by *horizontal* transitions in the graph and only reflect the passing of time as no changes to the physical hardware are made.

Conversely, diagonal transitions imply physical hardware changes because they represent decisions where chargers connect to or disconnect from a bus. One such example from figure 5 includes the edge from $n_{0,0}$ to $n_{1,1}$. The state represented by $n_{0,0}$ is disconnected This edge represents an interval where a charger is disconnected at t_0 and connected at t_1, implying a 'to-connect' decision. The same logic applies in reverse for the edge between $n_{1,2}$ and $n_{0,3}$. Hence, the bus charge problem can be described in terms of nodes and edges where nodes represent bus availability and edges encode all possible charge decisions.

A charge schedule can be thought of as a list of charge decisions that govern charge behavior. Because decisions are represented by edges in the graph, a schedule is also represented by a sequence of connected edges that form a path through the graph. If an edge is selected, or active, it is considered part of the path. Active and inactive edges are respectively represented edge weights equal to 1, and 0.

A graph with binary edge weights can only represent a plan for one charger. This representation can be expanded to represent an arbitrary number of chargers by using integer valued weights, where each weight gives the number of chargers in the transition.

Consider a three-charger scenario using the graph in figure 4. A solution where one charger is connected to Bus 1 from t_1 to t_2 and to Bus 2 from t_4 to t_5 would be expressed by assigning unit weights to the appropriate connect, charge, and disconnect edges. The second charger remains idle as illustrated by the active edges along the bottom row of charger states (see figure 6).

In summary, the graph encodes bus availability with nodes, decisions with edges, and schedules with edge weights. Solving the bus charge problem becomes a matter of finding the optimal set of edge weights, where optimal is used to denote the most cost effective charge plan.

B. MILP Constraints

Finding the optimal charge schedule can be expressed as an optimization problem, where the graph is encoded through equality/inequality constraints for a Mixed Integer Linear Program. This subsection formulates two sets of constraints. The first encodes the graph, enforces conservation of chargers, and defines the number of chargers through a set of net-flow constraints. The second prevents the charger from reconnecting shortly after disconnecting, and allows only a single charger to connect at a time by enforcing group-flow constraints.

1) Net-Flow Constraints:

$$Ax = c_f, \tag{1}$$

where A is the graph incidence matrix, x is an nEdge $\times$ 1 vector of edge weights, and c_f is nNode $\times$ 1 and equals the difference between incoming and outgoing edge weights, or *net-flow*.

An incidence matrix organizes relationships between nodes and edges by describing which edges leave and enter which

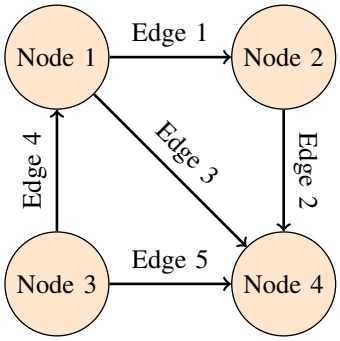

Fig. 7: A generic directed graph consisting of nodes and edges

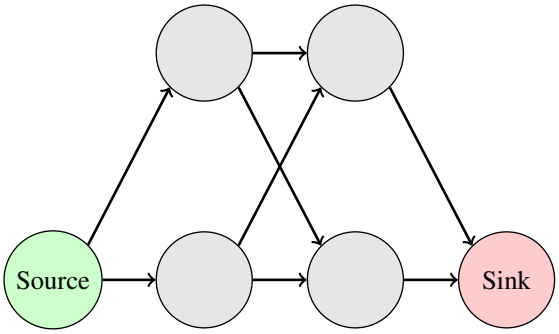

Fig. 8: Network flow illustrating sources and sinks

nodes. The matrix A is an nNode $\times$ nEdge matrix and expresses incoming connections between the i^{th} node and j^{th} edge as $A_{i,j} = 1$. Similarly, outgoing connections are given with $A_{i,j} = -1$, and no connection with $A_{i,j} = 0$. For example, the graph in figure 7 is represented as:

$$\begin{bmatrix} -1 & 0 & -1 & 1 & 0 \\ 1 & -1 & 0 & 0 & 0 \\ 0 & 0 & 0 & -1 & -1 \\ 0 & 1 & 1 & 0 & 1 \end{bmatrix} \tag{2}$$

The difference between the number of chargers entering and leaving, or the *net-flow*, can be expressed in terms of A as seen in equation 1. Because the number of chargers must be conserved, the number of incoming and outgoing chargers must be equal. This is expressed in linear form as $a_i^T x = 0$, where a_i is the i^{th} row of A. The only exceptions occur at *source* and *sink* nodes.

A source node represents the beginning state for all chargers. Because edges originate here, there are no incoming edges and the net-flow will be minus the number of chargers. This is described in linear form as $a_i^T x = -\text{nCharger}$.

Sink nodes represent the final state, where all edges terminate (see figure 8). Because sinks have no outgoing edges, they maintain a positive net-flow equal to the number of chargers and is expressed as $a_i^T = \text{nCharger}$.

Therefore, the *flow constraints* require that c_f be equal to zero for all non-source and non-sink nodes as seen in equation 3.

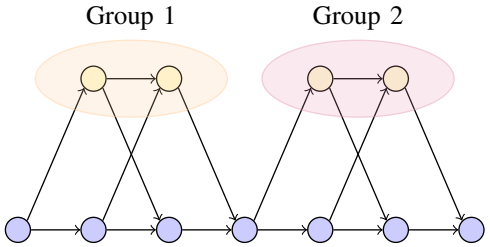

Fig. 9: Example of groups in a network flow graph

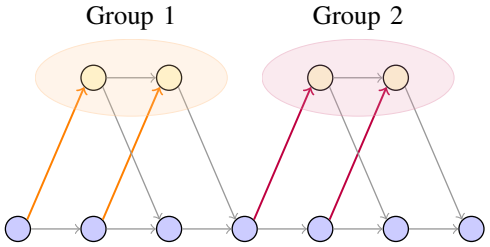

Fig. 10: Incoming Group Edges

$$Ax = \begin{bmatrix} 0 \\ \vdots \\ -\text{nCharger} \\ \vdots \\ 0 \\ \text{nCharger} \\ \vdots \\ 0 \end{bmatrix} \tag{3}$$

2) Group-flow Constraints: Another flow type, known as group flow, can be used to regulate the number of chargers entering a set of nodes. This is desired for two reasons: It avoids multiple reconnects during a charge period, and limits the number of connecting chargers to one.

Define a charge group as the set of all nodes for a given bus corresponding to one station visit as shown in figure 9. The *group flow* is the number of chargers that enter a group and is represented as the sum of all incoming edge weights (see figure 10).

Denote the nGroup $\times$ nEdge group incidence matrix as B, where $B_{i,j}$ is 1 if the j^{th} edge enters the i^{th} group and 0 otherwise. For example, the group incidence matrix corresponding to the graph in figure 11 contains 1 in the 7^{th} and 10^{th} columns for Group 1, and the 12^{th} and 15^{th} columns for group 2 as given in equation 4.

$$B = \begin{bmatrix} 0\,0\,0\,0\,0\,0\,1\,0\,0\,1\,0\,0\,0\,0\,0 \\ 0\,0\,0\,0\,0\,0\,0\,0\,0\,0\,1\,0\,0\,1\,0 \end{bmatrix} \tag{4}$$

Let x be the edge weights as before and c_g be an nGroup $\times$ 1 vector where the i^{th} element gives the group flow for group i. The group flow is then computed as

$$Bx = c_g \tag{5}$$

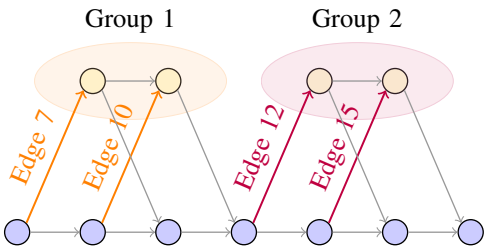

Fig. 11: Connect edge example for groups

But the group flow is required to be one at most to avoid thrashing. This is expressed by the inequality given in equation 6.

$$Bx \leq \begin{bmatrix} 1 \\ 1 \\ \vdots \\ 1 \end{bmatrix}. \tag{6}$$

C. Section Summary

In summary, the bus charge problem can be formulated as a graph with nodes and edges, where charge plans are encoded as a path. The charge problem aims to find a feasible path which minimizes the cost of power. Feasibility is defined through a set of net-flow and group-flow constraints. Net-flow constraints are encoded through an adjacency matrix and enforce both the conservation and total number of chargers. The group-flow constraints prevent charge thrashing and regulate the number of simultaneous charger-to-bus connections.

IV. Battery State of Charge

Battery state of charge (SOC) plays a role in the bus charge problem. Battery charge levels decrease as a bus traverses a route. Solutions to the bus charge problem account for routes and require that SOC values remain above a minimum threshold.

A SOC thresholding constraint requires that battery charge levels be estimated. The k^{th} SOC for bus i is denoted $d_{i,k}$, where k is the *node index*. Node indices are time agnostic such that $d_{i,k+1}$ represents the SOC bus node following $d_{i,k}$ as seen in figure 13.

Because no charging is performed while on route, $d_{i,k}$ will be lowest as buses enter the charge station. Let $d_{i,k+1}$ be the charge level for bus i as it enters the charge station, and δ_i represent the power discharged while on-route. The entrance SOC can be expressed as

$$d_{i,k+1} = d_{i,k} - \delta_i, \tag{7}$$

where $d_{i,k}$ is the previous departure SOC for bus i. Consider the example in figure 12, where buses 1 and 2 leave the station at t_2 and enter at t_4. The corresponding change in SOC is given as $d_{1,2} = d_{1,1} - \delta_1$ and $d_{2,2} = d_{2,1} - \delta_2$ for buses 1 and 2 respectively. The constraints from equation 7 can be expressed in linear standard form as

$$\begin{bmatrix} -1_{d_{i,k}} & 1_{d_{i,k+1}} \end{bmatrix} \begin{bmatrix} d_{i,k} \\ d_{i,k+1} \end{bmatrix} = \delta_i. \tag{8}$$

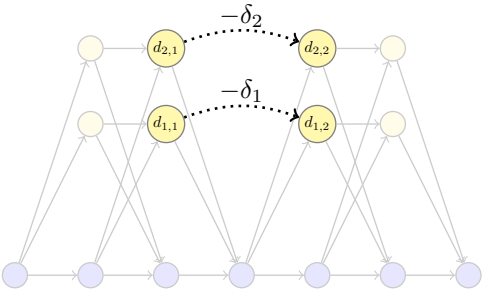

Fig. 12: Relationship between exit nodes (left) and entrance nodes (right) as δ

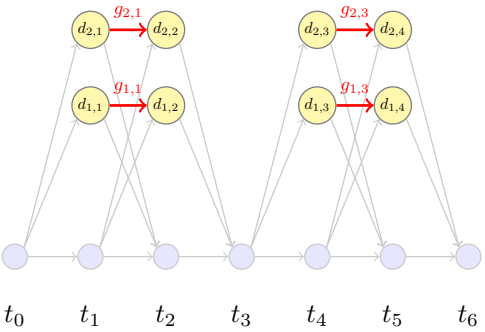

Fig. 13: Depiction of which edges increase SOC for the single rate case

Equation 8 can be expressed in terms of $\mathbf{y}$ with appropriate zero padding and expanded to account for the decrease in SOC for all buses outside the station. The expanded constraint is given as

$$D_\delta \mathbf{y} = \mathbf{d}_\delta. \tag{9}$$

Time periods between entrance and exit nodes represent time spent in the charge station and have the potential to charge the battery. An edge over which charging occures is refered to as $x_{i,k}$, where k gives the index of the edge's outgoing node, and i refers to the bus. When a charger occupies $x_{i,k}$, the resulting increase, or *gain*, in battery charge is denoted $g_{i,k}$, where i and k mirror the edge indices (see figure 13).

The value for $g_{i,k}$ is computed using a single charge rate. Additional flexibility can be encoded be connecting bus nodes with multiple edges, denoted $x_{i,k,l}$. Each edge has a distinct charge rate and gain denoted $g_{i,k,l}$ and together, the set of edges allows for multi-rate charging (see figure 14). Having multiple charge rates gives the option for fast charging when necessary, and slow charging when possible to preserve battery health and decrease the electrical load [9].

The rate is selected by setting $x_{i,k,l} = 1$. All gains associated with unselected rates are equal to zero. Gains that correspond to selected rates are computed using the Constant Current Constant Voltage (CCCV) model as derived in [19] which gives:

$$d_{i,k+1} = \bar{a}_l d_{i,k} - \bar{b}_l M, \tag{10}$$

where $\bar{a}_l \sim (0, 1]$, depends on the charge rate and is experimentally determined, M is the battery charge capacity in kWh,

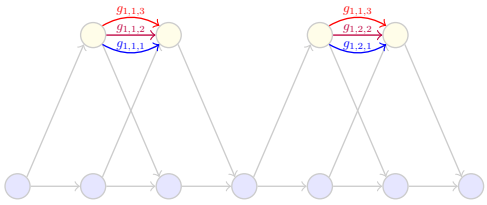

Fig. 14: Multi-Rate Charging

and $\bar{b}_l = \bar{a}_l - 1$. Equation 10 is used to show that

$$\begin{aligned} d_{i,k+1} &= \bar{a}_l d_{i,k} - \bar{b}_l M \\ d_{i,k+1} - d_{i,k} &= \bar{a}_l d_{i,k} - \bar{b}_l M - d_{i,k}, \end{aligned} \tag{11}$$

but the gain is equal to the difference in $d_{i,k+1}$ and $d_{i,k}$ such that $g_{i,k,l} = d_{i,k+1} - d_{i,k}$. So

$$\begin{aligned} g_{i,k,l} &= \bar{a}_l d_{i,k} - \bar{b}_l M - d_{i,k} \\ g_{i,k,l} &= (\bar{a}_l - 1) d_{i,k} - \bar{b}_l M. \end{aligned} \tag{12}$$

Therefore,

$$\begin{cases} g_{i,k,l} = d_{i,k}(\bar{a}_l - 1) - \bar{b}_l M & x_{i,k,l} = 1 \\ g_{i,k,l} = 0 & x_{i,k,l} = 0 \end{cases}. \tag{13}$$

The conditions given in equation 13 can be rewritten as

$$\begin{aligned} &\begin{cases} g_{i,k,l} \leq d_{i,k}(\bar{a}_l - 1) - \bar{b}_l M \\ g_{i,k,l} \geq d_{i,k}(\bar{a}_l - 1) - \bar{b}_l M \end{cases} && x_{i,k,l} = 1 \\ &\begin{cases} g_{i,k,l} \leq 0 \\ g_{i,k,l} \geq 0 \end{cases} && x_{i,k,l} = 0 \\ \Rightarrow\ & g_{i,k,l} \leq d_{i,k}(\bar{a}_l - 1) - \bar{b} M - M(1 - x_{i,k,l}) \\ & g_{i,k,l} \geq d_{i,k}(\bar{a}_l - 1) - \bar{b} M \\ & g_{i,k,l} \leq 0 + M x_{i,k,l} \\ & g_{i,k,l} \geq 0, \end{aligned} \tag{14}$$

where M is the battery capacity. The results of equation 14 obtain a switching effect. When $x_{i,k,l} = 1$, equation 14 becomes

$$\begin{aligned} &\left.\begin{aligned} g_{i,k,l} &\leq d_{i,k}(\bar{a}_l - 1) - \bar{b}_l M \\ g_{i,k,l} &\geq d_{i,k}(\bar{a}_l - 1) - \bar{b}_l M \end{aligned}\right\} \text{Active} \\ &\left.\begin{aligned} g_{i,k,l} &\leq M \\ g_{i,k,l} &\geq 0 \end{aligned}\right\} \text{Inactive} \end{aligned} \tag{15}$$

The active constraints imply equality for $g_{i,k,l} = (\bar{a}_l - 1) d_{i,k} - \bar{b}_l M$. The inactive constraints imply that $g_{i,k,l}$ is greater then zero and less then the battery capacity, which are trivially satisfied. When $x_{i,k,l} = 0$, equation 14 becomes

$$\begin{aligned} &\left.\begin{aligned} g_{i,k,l} &\leq d_{i,k}(\bar{a}_l - 1) - \bar{b}_l M - M \\ g_{i,k,l} &\geq d_{i,k}(\bar{a}_l - 1) - \bar{b}_l M \end{aligned}\right\} \text{Inactive} \\ &\left.\begin{aligned} g_{i,k,l} &\leq 0 \\ g_{i,k,l} &\geq 0 \end{aligned}\right\} \text{Active} \end{aligned} \tag{16}$$

Where the inactive constraints are again trivially satisfied, and the active imply equality for $g_{i,k,l} = 0$.

Equation 14 can be expressed in standard form as

$$\begin{aligned} -g_{i,k,l} + d_{i,k}(\bar{a}_l - 1) + x_{i,k,l} &\leq M(\bar{b}_l + 1) \\ g_{i,k,l} - d_{i,k}(\bar{a}_l - 1) &\leq -\bar{b}_l M \\ g_{i,k,l} - M x_{i,k,l} &\leq 0 \\ -g_{i,k,l} &\leq 0 \end{aligned} \tag{17}$$

and in matrix form as

$$\begin{bmatrix} -1 & \bar{a}_l - 1 & 1 \\ 1 & 1 - \bar{a}_1 & 0 \\ 1 & 0 & -M \\ -1 & 0 & 0 \end{bmatrix} \begin{bmatrix} g_{i,k,l} \\ d_{i,k} \\ x_{i,k,l} \end{bmatrix} \leq \begin{bmatrix} M(\bar{b}_l + 1 \\ -\bar{b}_l M \\ 0 \\ 0 \end{bmatrix}. \tag{18}$$

Equation 18 can be expanded to include constraints for all $g_{i,k,l}$. Becuase each value for $g_{i,k,l}$, $d_{i,k}$, and $x_{i,k,l}$ is an element of $\mathbf{y}$, the constraints from equation 18 can be written as

$$G\mathbf{y} \leq \mathbf{b}_g. \tag{19}$$

The value of $d_{i,k}$ can be expressed as

$$d_{i,k+1} = d_{i,k} + \sum_l g_{i,k,l} \tag{20}$$

or

$$d_{i,k+1} - d_{i,k} - \sum_l g_{i,k,l} = 0 \tag{21}$$

because a non-zero element of $g_{i,k,l}$ is only present for one corresponding l. This relationship is described in terms of an equality constraints such that

$$\begin{bmatrix} 1 & -1 & \dots & -1 \end{bmatrix} \begin{bmatrix} d_{i,k+1} \\ d_{i,k} \\ g_{i,k,1} \\ \dots \\ g_{i,k,l} \end{bmatrix} = 0. \tag{22}$$

Equation 22 can be appropriatly zero padded such that

$$\begin{bmatrix} 1_{d_{i,k+1}} & -1_{d_{i,k}} & \dots & -1_{g_{i,k,l}} \end{bmatrix} \mathbf{y} = 0. \tag{23}$$

and expanded to define the values for all $d_{i,k} \ni k > 0$ as

$$D_d \mathbf{y} = \mathbf{0}. \tag{24}$$

The values for $d_{i,0}$ are defined with initial SOC conditions with additional equality constraints, denoted $\mathbf{d}_0$ such that

$$\begin{bmatrix} 1_{d_{1,0}} & 0 & 0 & \dots & 0 \\ 0 & \dots & 1_{d_{2,0}} & 0 & 0 \\ \vdots & & \vdots & & \vdots \\ 0 & 0 & 0 & \dots & 1_{d_{i,0}} \end{bmatrix} \mathbf{y} = \mathbf{d}_0, \tag{25}$$

or

$$D_0 \mathbf{y} = \mathbf{d}_0. \tag{26}$$

Once all values for $d_{i,k}$ are computed, they must be constrainted to remain above a threshold τ. The SOC thresholing constraint can be expessed as an inequality constraint such that

$$\begin{aligned} & d_{i,k} \geq \tau \\ \Rightarrow & -d_{i,k} \leq -\tau \\ \Rightarrow & \begin{bmatrix} 0 & \dots & -1_{d_{i,k}} & \dots & 0 \end{bmatrix} \mathbf{y} \leq -\tau \end{aligned} \tag{27}$$

Equation 27 can be expanded to a matrix D_τ, where each each $d_{i,k}$ contains a corresponding constraint row such that

$$D_\tau \mathbf{y} \leq \begin{bmatrix} -\tau \\ \vdots \\ -\tau \end{bmatrix} \leq \mathbf{d}_\tau \tag{28}$$

In summary, the minimum SOC for all feasible charge plans must exceed a given threshold. SOC values are computed while the bus is in the charge station. SOC values are updated when a bus enters by subtracting the discharged energy from the previous SOC estimate. SOC values are updated for in-station periods by adding the charge gains as given in equation 20. Gains are computed using a switching constraint which sets them to zero when not charging, otherwise they follow the CCCV model as derived in equation 12. Initial SOC values are handled with the equality constraint given in equation 26 and the SOC is constrained to remain above the threshold τ in equation 28. All constraints for d can be concatenated such that

$$\begin{bmatrix} D_0 \\ D_\delta \\ D_d \end{bmatrix} \mathbf{y} = \begin{bmatrix} \mathbf{d}_0 \\ \mathbf{d}_\delta \\ \mathbf{0} \end{bmatrix}, \quad \begin{bmatrix} D_g \\ D_\tau \end{bmatrix} \mathbf{y} \leq \begin{bmatrix} \mathbf{d}_g \\ \mathbf{d}_\tau \end{bmatrix} \tag{29}$$

and expressed as

$$D_{\text{eq}}\mathbf{y} = \mathbf{d}_{\text{eq}}, \quad D_{\text{ineq}}\mathbf{y} \leq \mathbf{d}_{\text{ineq}} \tag{30}$$

V. Multi-Graph Additions

An additional contribution this work offers is the expansion to night vs day charging. Day and night operations differ in two aspects: number of chargers, and bus availability. During the day, the buses can charge on chargers in the charge station. The number of chargers in the station are limited, causing contention between buses. At night, each bus docks in a holding stall with one charger per stall, eliminating charger contention.

Bus availability also changes because buses do not leave their stalls at night. This simplifies the charge problem because buses are always available for charging.

Equation 3 in section III-B1 describes the net-flow constraints which constrain the number of chargers in the source and sink nodes. Because the number of chargers are different from night to day, a separate graph is used at each transition as shown in figure 15.

Each graph is connected by equating the appropriate SOC values. Consider the multi-graph formulation given in figure 16. The morning graph is related to the day graph because $d_{1,1}$ and $d_{2,1}$ represent the same SOC values as $d_{1,2}$ and $d_{2,2}$ respectively. The same applies for the day and night graph, where $d_{1,5}$ and $d_{2,5}$ represent the SOC values for $d_{1,6}$ and $d_{2,6}$. This equality relationship can be expressed as an equality constraint where

$$\mathbf{d}_{\text{graph 1}} - \mathbf{d}_{\text{graph 2}} = \mathbf{0} \tag{31}$$

or by

$$D_{\text{multi-graph}}\mathbf{y} = \mathbf{0}, \tag{32}$$

where $D_{\text{multi-graph}}$ is an nBus $\times$ nVar matrix such that

$$D_{\text{multi-graph}}\mathbf{y} = \mathbf{d}_{\text{graph 1}} - \mathbf{d}_{\text{graph 2}}. \tag{33}$$

Because all SOC values d are contained in $\mathbf{y}$, forming the matrix D amounts to placing 1 and -1 at the indices corresponding to $d_{\text{graph 1}}$ and $d_{\text{graph 2}}$ respectively and zero otherwise.

VI. Objective Function

The objective function in this work models the rate schedule used in [16], where the result is modeled as the monthly charge a transit authority might receive from the power provider. The objective function includes charges for energy, power, and facility use and implements both on and off-peak rates.

A. Energy

Energy charges are given per Kilowatt-hour of energy consumed and include power from external loads and bus chargers. Let $\mathbf{p}$ be the average external power used at each timestep, where $\mathbf{p}_i$ is the average power draw between t_j and t_{j+1}. The energy consumed by external loads from t_j to t_{j+1} is computed as

$$e_{l_j} = \mathbf{p}_i \times \Delta_t, \tag{34}$$

where Δ_t is the change in time from t_j to t_{j+1} in hours. The energy consumed by bus chargers for the same interval is computed as

$$e_{b_j} = \sum_{k \in t} g_{i,k,l}, \tag{35}$$

which sums all changes in bus SOC between t_j and t_{j+1}. The total energy is computed as

$$e_j = e_{l_j} + e_{b_j} \tag{36}$$

The equation for 36 can be written in standard form as

$$\begin{aligned} e_j - \sum_{k \in t} g_{i,k,l} &= p_i \times \Delta_t \\ \begin{bmatrix} 1_{e_j} & -1_{g_1} & \dots -1_{g_n} \end{bmatrix} \begin{bmatrix} e_j \\ g_1 \\ \vdots \\ g_n \end{bmatrix} &= p_i \times \Delta_t \end{aligned} \tag{37}$$

Equation 37 can be modified to reflect the energy consumed in an arbitrary time period, T, by including the corresponding values for g and p as

$$\begin{aligned} e_T - \sum_{k \in T} g_{i,k,l} &= \left(\sum_{i \in T} p_i \right) \times \Delta_t \\ \begin{bmatrix} 1_{e_j} & -1_{g_1} & \dots -1_{g_n} \end{bmatrix} \begin{bmatrix} e_j \\ g_1 \\ \vdots \\ g_n \end{bmatrix} &= p_T \times \Delta_t. \end{aligned} \tag{38}$$

For multiple time periods, the constraint can be expanded in matrix form, where row i corresponds to the periods of time in T_i. Furthermore, by including e_j in the solution vector $\mathbf{y}$ and

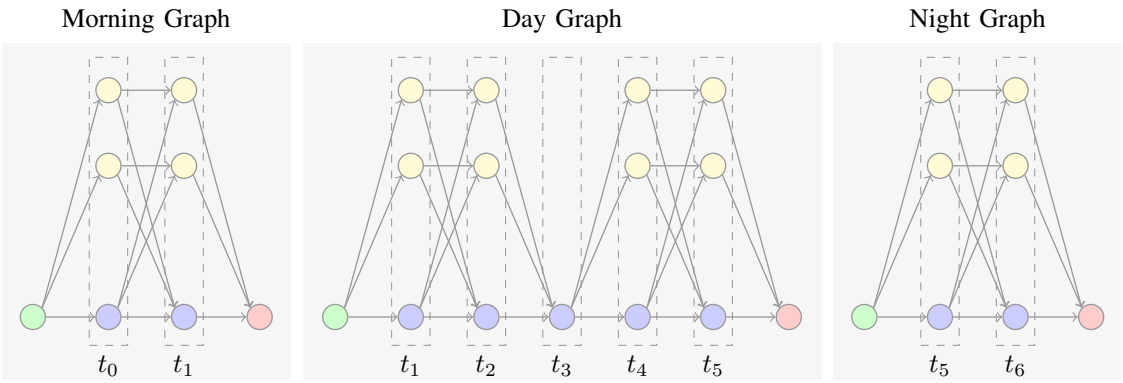

Fig. 15: Night and Day Graphs

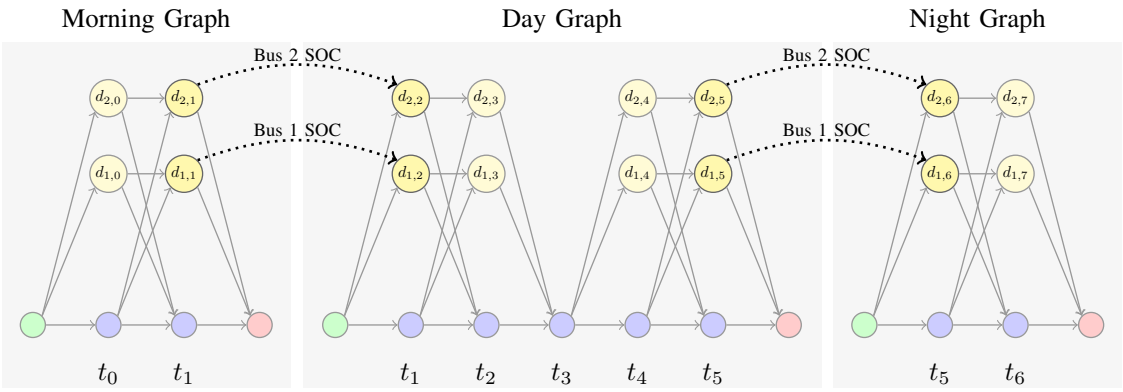

Fig. 16: Bus SOC between Night and Day Graphs

zero-padding appropriately, the expanded form of equation 38 can be written as

$$E\mathbf{y} = \mathbf{e}_p, \tag{39}$$

where row i in E reflects equation 38 for the time intervals in T_i, and $\mathbf{e}_{p_i}$ contains the energy from external loads during T_i. The day is divided into on and off-peak times. on-peak times reflect periods where high power use is common.

B. Power

Power charges are computed for the maximum average power draw, where the average is computed over a 15 minute sliding window. The average power can be computed as the energy in the window divided by the window length in hours. In this case, a 15 minute window equates to a quarter hour. Let $\bar{p}_j$ be the average power from $j-15$ to j. Equation 38 can be adapted to compute the average power as

$$\begin{gathered}\bar{p}_j - \left(\sum_{k\in T_j} g_{i,k,l}\right)/4 = \left(\sum_{i\in T_j} p_i\right) \times \frac{\Delta_t}{4} \\ \begin{bmatrix} 1_{\bar{p}_j} & -\frac{1_{g_1}}{4} & \dots & -\frac{1_{g_n}}{4} \end{bmatrix} \begin{bmatrix} e_j \\ g_1 \\ \vdots \\ g_n \end{bmatrix} = \frac{p_T \times \Delta_t}{4}.\end{gathered} \tag{40}$$

Equation 40 can further be expanded and zero padded to compute the average power at each time, t_i by applying equation 40 to the corresponding window as

$$P\mathbf{y} = \mathbf{p}. \tag{41}$$

The maximum average power, denoted $\bar{p}_{\text{max}}$, is greater than or equal to each average power computed in equation 41. This yields an additional set of inequality constraints

$$\begin{gathered}\begin{bmatrix} -1_{\hat{p}} & 1_{p_0} & 0 & \dots & 0 \\ -1_{\hat{p}} & 0 & 1_{\bar{p}_1} & \dots & 0 \\ -1_{\hat{p}} & 0 & 0 & \dots & 1_{\bar{p}_j} \end{bmatrix} \leq \mathbf{0} \\ P_{\text{max}} \leq \mathbf{0}.\end{gathered} \tag{42}$$

Because the max average power is minimizied in the objective function, the value for $\hat{p}_{\text{max}}$ will be forced down to the value of the greatest average power computed in equation 41, and accurately reflect the maximum average power.

C. On/Off Peak Rates

D. Objective Function

VII. Results

VIII. Future Work

REFERENCES

[1] Avishan Bagherinezhad et al. "Spatio-Temporal Electric Bus Charging Optimization With Transit Network Constraints". In: *IEEE Transactions on Industry Applications* 56.5 (Sept. 2020), pp. 5741–5749. ISSN: 0093-9994, 1939-9367. DOI: 10.1109/TIA.2020.2979132. URL: https://ieeexplore.ieee.org/document/9028116/ (visited on 11/13/2021).

[2] Bhagyashree J Balde and Arghya Sardar. "Electric Road system With Dynamic Wireless charging of Electric buses". In: *2019 IEEE Transportation Electrification Conference (ITEC-India)*. 2019 IEEE Transportation Electrification Conference (ITEC-India). Bengaluru, India: IEEE, Dec. 2019, pp. 1–4. ISBN: 978-1-72813-169-6. DOI: 10.1109/ITEC-India48457.2019.ITECINDIA2019-251. URL: https://ieeexplore.ieee.org/document/9080859/ (visited on 11/18/2021).

[3] T. Boonraksa et al. "Impact of Electric Bus Charging on the Power Distribution System a Case Study IEEE 33 Bus Test System". In: *2019 IEEE PES GTD Grand International Conference and Exposition Asia (GTD Asia)*. 2019 IEEE PES GTD Grand International Conference and Exposition Asia (GTD Asia). Bangkok, Thailand: IEEE, Mar. 2019, pp. 819–823. ISBN: 978-1-5386-7434-5. DOI: 10.1109/GTDAsia.2019.8716023. URL: https://ieeexplore.ieee.org/document/8716023/ (visited on 11/13/2021).

[4] Qifu Cheng et al. "A smart charging algorithm-based fast charging station with energy storage system-free". In: *CSEE Journal of Power and Energy Systems* (2020). ISSN: 20960042, 20960042. DOI: 10.17775/CSEEJPES.2020.00350. URL: https://ieeexplore.ieee.org/stamp/stamp.jsp?tp=&arnumber=9171658 (visited on 11/19/2021).

[5] Blint Csonka. "Optimization of Static and Dynamic Charging Infrastructure for Electric Buses". In: *Energies* 14.12 (June 13, 2021), p. 3516. ISSN: 1996-1073. DOI: 10.3390/en14123516. URL: https://www.mdpi.com/1996-1073/14/12/3516 (visited on 11/13/2021).

[6] Sanchari Deb, Karuna Kalita, and Pinakeshwar Mahanta. "Impact of electric vehicle charging stations on reliability of distribution network". In: *2017 International Conference on Technological Advancements in Power and Energy (TAP Energy)*. 2017 International Conference on Technological Advancements in Power and Energy (TAP Energy). Kollam: IEEE, Dec. 2017, pp. 1–6. ISBN: 978-1-5386-4021-0. DOI: 10.1109/TAPENERGY.2017.8397272. URL: https://ieeexplore.ieee.org/document/8397272/ (visited on 11/16/2021).

[7] Nader A. El-Taweel and Hany E. Z. Farag. "Incorporation of Battery Electric Buses in the Operation of Intercity Bus Services". In: *2019 IEEE Transportation Electrification Conference and Expo (ITEC)*. 2019 IEEE Transportation Electrification Conference and Expo (ITEC). Detroit, MI, USA: IEEE, June 2019, pp. 1–6. ISBN: 978-1-5386-9310-0. DOI: 10.1109/ITEC.2019.8790598. URL: https://ieeexplore.ieee.org/document/8790598/ (visited on 11/19/2021).

[8] Qiang Gao et al. "Charging Load Forecasting of Electric Vehicle Based on Monte Carlo and Deep Learning". In: *2019 IEEE Sustainable Power and Energy Conference (iSPEC)*. 2019 IEEE Sustainable Power and Energy Conference (iSPEC). Beijing, China: IEEE, Nov. 2019, pp. 1309–1314. ISBN: 978-1-72814-930-1. DOI: 10.1109/iSPEC48194.2019.8975364. URL: https://ieeexplore.ieee.org/document/8975364/ (visited on 11/19/2021).

[9] Adnane Houbbadi et al. "Optimal Charging Strategy to Minimize Electricity Cost and Prolong Battery Life of Electric Bus Fleet". In: *2019 IEEE Vehicle Power and Propulsion Conference (VPPC)*. 2019 IEEE Vehicle Power and Propulsion Conference (VPPC). Hanoi, Vietnam: IEEE, Oct. 2019, pp. 1–6. ISBN: 978-1-72811-249-7. DOI: 10.1109/VPPC46532.2019.8952493. URL: https://ieeexplore.ieee.org/document/8952493/ (visited on 11/13/2021).

[10] Amra Jahic, Mina Eskander, and Detlef Schulz. "Preemptive vs. non-preemptive charging schedule for large-scale electric bus depots". In: *2019 IEEE PES Innovative Smart Grid Technologies Europe (ISGT-Europe)*. 2019 IEEE PES Innovative Smart Grid Technologies Europe (ISGT-Europe). Bucharest, Romania: IEEE, Sept. 2019, pp. 1–5. ISBN: 978-1-5386-8218-0. DOI: 10.1109/ISGTEurope.2019.8905633. URL: https://ieeexplore.ieee.org/document/8905633/ (visited on 11/16/2021).

[11] Shubham Jain et al. "Battery Swapping Technology". In: *2020 5th IEEE International Conference on Recent Advances and Innovations in Engineering (ICRAIE)*. 2020 5th IEEE International Conference on Recent Advances and Innovations in Engineering (ICRAIE). Jaipur, India: IEEE, Dec. 1, 2020, pp. 1–4. ISBN: 978-1-72818-867-6. DOI: 10.1109/ICRAIE51050.2020.9358366. URL: https://ieeexplore.ieee.org/document/9358366/ (visited on 11/18/2021).

[12] Seog Y. Jeong et al. "Automatic Current Control by Self-Inductance Variation for Dynamic Wireless EV Charging". In: *2018 IEEE PELS Workshop on Emerging Technologies: Wireless Power Transfer (Wow)*. 2018 IEEE PELS Workshop on Emerging Technologies: Wireless Power Transfer (WoW). Montral, QC, Canada: IEEE, June 2018, pp. 1–5. ISBN: 978-1-5386-2465-4. DOI: 10.1109/WoW.2018.8450926. URL: https://ieeexplore.ieee.org/document/8450926/ (visited on 11/18/2021).

[13] Inaki Ojer et al. "Development of energy management strategies for the sizing of a fast charging station for electric buses". In: *2020 IEEE International Conference on Environment and Electrical Engineering and 2020 IEEE Industrial and Commercial Power Systems Europe (EEEIC / I&CPS Europe)*. 2020 IEEE International Conference on Environment and Electrical Engineering and 2020 IEEE Industrial and Commercial Power Systems Europe (EEEIC / I&CPS Europe). Madrid, Spain:

IEEE, June 2020, pp. 1–6. ISBN: 978-1-72817-455-6. DOI: 10.1109/EEEIC/ICPSEurope49358.2020.9160716. URL: https://ieeexplore.ieee.org/document/9160716/ (visited on 11/16/2021).

[14] Kavuri Poornesh, Kuzhivila Pannickottu Nivya, and K. Sireesha. "A Comparative study on Electric Vehicle and Internal Combustion Engine Vehicles". In: *2020 International Conference on Smart Electronics and Communication (ICOSEC)*. 2020 International Conference on Smart Electronics and Communication (ICOSEC). Trichy, India: IEEE, Sept. 2020, pp. 1179–1183. ISBN: 978-1-72815-461-9. DOI: 10.1109/ICOSEC49089.2020.9215386. URL: https://ieeexplore.ieee.org/document/9215386/ (visited on 11/13/2021).

[15] Nan Qin et al. "Numerical analysis of electric bus fast charging strategies for demand charge reduction". In: *Transportation Research Part A: Policy and Practice* 94 (Dec. 2016), pp. 386–396. ISSN: 09658564. DOI: 10.1016/j.tra.2016.09.014. URL: https://linkinghub.elsevier.com/retrieve/pii/S096585641630444X (visited on 11/13/2021).

[16] *Rocky Mountain Power Electric Service Schedule No. 8 State of Utah*. URL: https://www.rockymountainpower.net/content/dam/pcorp/documents/en/rockymountainpower/rates-regulation/utah/rates/008_Large_General_Service_1_000_kW_and_Over_Distribution_Voltage.pdf (visited on 02/03/2022).

[17] Daniel Stahleder et al. "Impact Assessment of High Power Electric Bus Charging on Urban Distribution Grids". In: *IECON 2019 - 45th Annual Conference of the IEEE Industrial Electronics Society*. IECON 2019 - 45th Annual Conference of the IEEE Industrial Electronics Society. Lisbon, Portugal: IEEE, Oct. 2019, pp. 4304–4309. ISBN: 978-1-72814-878-6. DOI: 10.1109/IECON.2019.8927526. URL: https://ieeexplore.ieee.org/document/8927526/ (visited on 11/16/2021).

[18] Ran Wei et al. "Optimizing the spatio-temporal deployment of battery electric bus system". In: *Journal of Transport Geography* 68 (Apr. 2018), pp. 160–168. ISSN: 09666923. DOI: 10.1016/j.jtrangeo.2018.03.013. URL: https://linkinghub.elsevier.com/retrieve/pii/S0966692317306294 (visited on 11/13/2021).

[19] Justin Whitaker et al. "A Network Flow Approach to Battery Electric Bus Scheduling". In: (2021), p. 10.

[20] Xian Zhang and Guibin Wang. "Optimal dispatch of electric vehicle batteries between battery swapping stations and charging stations". In: *2016 IEEE Power and Energy Society General Meeting (PESGM)*. 2016 IEEE Power and Energy Society General Meeting (PESGM). Boston, MA, USA: IEEE, July 2016, pp. 1–5. ISBN: 978-1-5090-4168-8. DOI: 10.1109/PESGM.2016.7741893. URL: http://ieeexplore.ieee.org/document/7741893/ (visited on 11/18/2021).

[21] Dan Zhou et al. "Optimization Method of Fast Charging Buses Charging Strategy for Complex Operating Environment". In: *2018 2nd IEEE Conference on Energy Internet and Energy System Integration (EI2)*. 2018 2nd IEEE Conference on Energy Internet and Energy System Integration (EI2). Beijing: IEEE, Oct. 2018, pp. 1–6. ISBN: 978-1-5386-8549-5. DOI: 10.1109/EI2.2018.8582378. URL: https://ieeexplore.ieee.org/document/8582378/ (visited on 11/13/2021).